Mechanistic analysis of iron accumulation by endothelial cells of the BBB

ARTICLE *in* BIOLOGY OF METALS · MARCH 2012

Impact Factor: 2.5 · DOI: 10.1007/s10534-012-9538-6 · Source: PubMed

2 AUTHORS:

Ryan C. McCarthy
Harvard University
8 PUBLICATIONS **76** CITATIONS
SEE PROFILE

Daniel J Kosman
University at Buffalo, The State Univer…
121 PUBLICATIONS **3,843** CITATIONS
SEE PROFILE

Biometals (2012) 25:665–675
DOI 10.1007/s10534-012-9538-6

Mechanistic analysis of iron accumulation by endothelial cells of the BBB

Ryan C. McCarthy · Daniel J. Kosman

Received: 19 December 2011 / Accepted: 4 March 2012 / Published online: 21 March 2012

Abstract The mechanism(s) by which iron in blood is transported across the blood–brain barrier (BBB) remains controversial. Here we have examined the first step of this trans-cellular pathway, namely the mechanism(s) of iron uptake into human brain microvascular endothelial cells (hBMVEC). We show that hBMVEC actively reduce non-transferrin bound Fe^{III} (NTBI) and transferrin-bound Fe^{III} (TBI); this activity is associated with one or more ferrireductases. Efficient, exo-cytoplasmic ferri-reduction from TBI is dependent upon transferrin receptor (TfR), also. Blocking holo-Tf binding with an anti-TfR antibody significantly decreases the reduction of iron from transferrin by hBMVEC, suggesting that holo-Tf needs to bind to TfR in order for efficient reduction to occur. Ferri-reduction from TBI significantly decreases when hBMVEC are pre-treated with Pt^{II}, an inhibitor of cell surface reductase activity. Uptake of ^{59}Fe from ^{59}Fe-Tf by endothelial cells is inhibited by 50 % when ferrozine is added to solution; in contrast, no inhibition occurs when cells are alkalinized with NH_4Cl. This indicates that the iron reduced from holo-transferrin at the plasma membrane accounts for at least 50 % of the iron uptake observed. hBMVEC-dependent reduction and uptake of NTBI utilizes a Pt^{II}-insensitive reductase. Reductase-independent uptake of Fe^{II} by hBMVEC is inhibited up to 50 % by Zn^{II} and/or Mn^{II} by a saturable process suggesting that redundant Fe^{II} transporters exist in the hBMVEC plasma membrane. These results are the first to demonstrate multiple mechanism(s) of TBI and NTBI reduction and uptake by endothelial cells (EC) of the BBB.

Keywords Blood–brain barrier · Iron · Neurodegeneration · Transferrin · Dcytb · STEAP2

Abbreviations

Asc	Ascorbic acid
BBB	Blood–brain barrier
BMVEC	Brain microvascular endothelial cells
CNS	Central nervous system
Dcytb	Duodenal cytochrome b
DMT1	Divalent metal transporter 1
EC	Endothelial cells
E°	Electrochemical potential
hBMVEC	Human brain microvascular endothelial cells
MVEC	Microvascular endothelial cells
NTBI	Non-transferrin bound iron
STEAP2	Six-transmembrane epithelial antigen of the prostate 2
TBI	Transferrin-bound iron
Tf	Transferrin
TfR	Transferrin receptor

Electronic supplementary material The online version of this article (doi:10.1007/s10534-012-9538-6) contains supplementary material, which is available to authorized users.

R. C. McCarthy · D. J. Kosman (✉)
Department of Biochemistry, SUNY University at Buffalo, School of Medicine and Biomedical Sciences, Buffalo, NY, USA
e-mail: camkos@buffalo.edu

Introduction

Iron, while required for several normal physiological processes, can be duplicitous in nature. Iron's innate ability to accept and donate electrons is vital for cellular processes such as mitochondrial energy generation, myelination, neurotransmission, oxygen transport, and cellular division (Salvador 2010; Madsen and Gitlin 2007). A disruption in the normal redox chemistry of brain iron can be detrimental to normal function. Improper iron regulation by cells of the brain has been linked to neurological disorders such as Alzheimer's and Parkinson's disease (Madsen and Gitlin 2007; Rivera-Mancía et al. 2010). To fully understand the pathology of these neurological diseases, we need to fully understand the mechanisms of iron transport into the brain, the cellular distribution/regulation of iron in the brain parenchyma and the mechanism(s) of iron efflux out of the central nervous system (CNS). Here, we focus in on the first of these steps; iron uptake by the capillary endothelial cells (EC) of the blood brain barrier (BBB).

The BBB is a unique entity which consists of microvascular endothelial cells (MVEC), glial cells, and pericytes all of which are thought to act as a single unit to protect the brain from harmful polar molecules. The endothelial cells of the BBB possess tight-junctions while lacking the fenestrations common to EC in the periphery; therefore, solutes in the blood must be transported transcellulary into the brain (Rouault and Cooperman 2006; Abbott et al. 2006).

Iron in the blood is coordinated to small molecule ligands such as citrate (Königsberger et al. 2000) (non-transferrin bound iron, NTBI) or to the iron transport protein Tf (transferrin bound iron, TBI). For endothelial cells to acquire iron from either TBI or NTBI, a luminal uptake mechanism must exist. Typically, uptake of TBI occurs when holo-Tf binds its receptor, followed by the release and reductase-dependent reduction of TBI in the endosome; this Fe^{II} is then exported from the endosome through a divalent cation transporter such as divalent metal transporter 1 (DMT1) (Rouault and Cooperman 2006; Garrick 2011). Previous studies have demonstrated the expression and co-localization of the iron-related transport proteins DMT1 and TfR in the brain microvasculature (Burdo et al. 2001; Yang et al. 2010; Siddappa et al. 2002), although the expression of DMT1 is controversial (Moos et al. 2007). A thorough examination of the divalent cations which act either as substrate or competitor of DMT1-mediated transport, has been reported (Garrick et al. 2006a). Such cations include but may not be limited to Mn^{II}, Cd^{II}, Fe^{II}, Pb^{II}, Co^{II}, Ni^{II}, Zn^{II}, and possibly Cu^{I} and/or Cu^{II}.

Recent reports indicate that transcripts expressing the ferrireductases duodenal cytochrome *b* (Dcytb) and six-transmembrane epithelial antigen of the prostate 2 (STEAP2) exist in the brain (Ohgami et al. 2006; Tulpule et al. 2010). Both of these ferrireductases catalyze the transport of electrons from cytosolic reductants [ascorbate or NAD(P)H] to extracellular or endosomal Fe^{III} (Ohgami et al. 2006; Atanasova et al. 2004). However, there are no literature reports demonstrating expression or functional reductase activity of either Dcytb or STEAP2 in brain MVEC (BMVEC).

To investigate the uptake mechanism(s) associated with EC accumulation of Fe from TBI and NTBI, we used monolayers of a human brain microvascular endothelial cell line (hBMVEC). Using this model system we examined the expression of iron-related transport proteins and their roles in iron reduction and uptake. We distinguish between TBI and NTBI reduction and assess the divalent metal ion uptake kinetic properties of the divalent cation transporter(s) in hBMVEC.

Materials and methods

Cell culture

hBMVEC were a generous gift from Dr. Supriya Mahajan at the Center for Innovation, Buffalo, NY. hBMVEC and Caco-2 cells were cultured in RPMI 1640 containing 1× MEM amino acids, 1× MEM vitamins (Mediatech Inc, Manassas, VA), 10 % FBS (Gemini Bio-products, West Sacramento, CA), 10 % NuSerum (BD Biosciences, Bedford, MA), 25 mM HEPES (Thermo Fisher Scientific, Waltham, MA), penicillin (100 U/mL), streptomycin (100 U/mL), 2 mM L-glutamine (Sigma-Aldrich, St. Louis, MO), 1 mM sodium pyruvate, heparin (5 U/mL) (Alfa Aesar, Ward Hill, MA), and $NaHCO_3$, pH 7.4. Cells were incubated in a humidified incubator at 37 °C, 5 % CO_2. The culture medium was replaced every other day and cells were passaged weekly. All experiments were performed in 24-well tissue culture dishes unless otherwise specified. Experiments were

performed between passage 4 and 8 when cells reached approximately 90–95 % confluency.

Indirect immunofluorescence

All indirect immunofluorescence incubations involved gentle agitation. Monolayers were washed 3× with 1 ml of phosphate-buffered saline (PBS) solution. The cells were then fixed for 10 min at room temperature (RT) with 3.7 % formaldehyde, and washed 4× with PBS (5 min/wash). Non-specific binding sites were blocked with 3 % bovine serum albumin (BSA) (EMD Chemicals, Darmstadt, Germany) in PBS at RT for 90 min. Cells were then incubated with primary antibody (1:1000 dilution of goat polyclonal anti-human TfR antibody (R&D Systems, Minneapolis, MN), mouse monoclonal anti-human VWF antibody, or goat polyclonal anti-STEAP2 antibody (Santa Cruz Biotechnology, Inc., Santa Cruz, CA)) in 3 % BSA in PBS over-night (O/N) at 4 °C. Cultures were then washed 3× with PBS, after which cells were incubated with secondary antibody (1:3,000 dilution of Alexa Fluor 488 donkey anti-goat IgG (Life Technologies, Grand Island, NY) (TfR & STEAP2), or Cy5 conjugated rabbit anti-mouse IgG (Jackson ImmunoResearch Laboratories, Inc., West Grove, PA) (VWF)) in 3 % BSA in PBS at RT for 1 h in the dark. The cells were then washed 3× with PBS in the dark at RT, after which they were imaged. Images were obtained using a Zeiss Axio Observer inverted microscope, 40× magnification and Zeiss AxioVision software (Zeiss, Thornwood, NY). The captured images were adjusted for brightness and contrast using Adobe Photoshop 7.0 software.

Immunoblots

Membrane proteins from Caco-2 and hBMVEC were separated from the cellular protein pool as follows. Cells were removed from 100 mm tissue culture dishes, washed 2× with PBS, and were pelleted. The cell pellet was resuspended with membrane purification buffer (50 mM Tris, 150 mM NaCl, pH 7.4) in a 5:1 ratio of buffer to pellet. Protease inhibitors were added to the cell suspension and the cells were cracked open by 3 rapid freeze–thaw cycles in liquid nitrogen and ice, respectively. The cell suspension was then centrifuged at 14,000×*g* for 30 min at 4 °C. The supernatant was removed leaving only membranes and membrane proteins in the pellet. This fraction was resuspended with a 1:1 ratio of mammalian lysis buffer plus protease inhibitors (100 mM HEPES, pH 7.4, 0.5 % (v/v) IGEPAL) to pellet and was stored O/N at 4 °C. For whole cell lysates, confluent monolayers of cells were lysed with mammalian lysis buffer plus protease inhibitors for 1 h 37 °C 5 % CO_2 110 rpm. Protein content was quantified and equal amounts of protein were run in each well of a 10 % SDS-PAGE for 20 min at 109 V followed by 180 V until the front ran off the gel. Proteins were transferred onto a PVDF membrane at 0.15 amps for 75 min using a semi-dry transfer apparatus. The PVDF membranes were blocked with 5 % BSA in TBST for 1 h at 4 °C. Membranes were then incubated with primary antibody (1:10,000 dilution of mouse monoclonal anti-DMT1 antibody (Acris Antibodies, San Diego, CA), 1:5,000 dilution of goat polyclonal anti-STEAP2 antibody, or 1:5,000 dilution of rabbit polyclonal anti-human Dcytb antibody (Acris Antibodies, San Diego, CA)) in TBST O/N at 4 °C. The anti-DMT1 antibody is specific for exon 2 so it is not isoform-specific. Membranes were washed for 1 h then incubated with secondary antibody (0.3 µl/ml of goat anti-rabbit IgG-HRP or donkey anti-goat IgG-HRP (Santa Cruz Biotechnology, Inc., Santa Cruz, CA) in TBST 3 % BSA for 1 h at RT. Membranes were washed for 1 h with TBST and then processed in a dark room using SuperSignal West Dura Extended Duration Substrate (Thermo Scientific, Waltham, MA) as per instructed. Films were scanned and the captured images were adjusted for brightness and contrast using Adobe Photoshop 7.0 software.

Pt^{II} cytotoxicity assay

All assays were performed using CytoTox 96 Non-Radioactive Cytotoxicity Assay from Promega (Promega Corporation, Madison, WI) as per instructions. Briefly, experiments were performed in triplicate under conditions mimicking the ferrozine assay. After a 3.5 h incubation, the supernatants were collected and assayed for LDH content. Percent cytotoxicity is calculated by dividing experimental LDH levels by total LDH times one hundred.

Colorimetric-based ferrozine assay for Fe^{II}

All assays were performed with a total working volume of 150 µl shaking at 100 rpm in a 37 °C 5 %

CO_2 humidified incubator. We used a physiological incubation buffer (PIB) for all assays (25 mM MOPS, 25 mM MES, 5.4 mM KCl, 5 mM glucose, 140 mM NaCl, 1.8 mM $CaCl_2$, 800 μM $MgCl_2$, pH 7.0). Final working concentrations of reagents (unless otherwise specified) were as follows: 10 μg/ml TfR-Ab, 25 μM Holo-Tf (EMD Chemicals, Darmstadt, Germany), 100 μM potassium tetrachloroplatinate^{II} (Pt^{II}) (Alfa Aesar, Ward Hill, MA), 100 μM $FeCl_3$ (Thermo Fisher Scientific, Waltham, MA), and 250 μM Citrate, 1 mM ferrozine, 250 μM apo-Tf from Sigma-Aldrich, St. Louis, MO. Each assay contained ferrozine and citrate (unless noted otherwise), plus the reagents indicated in the respective graph. All pre-incubations were conducted for 30 min after which the cells were washed with PBS and assay reagents were added and incubated for 3 h. After the 3 h incubation the PIB was collected and 50 μl was transferred to a 96-well plate. Absorbance readings were taken at 562 nm using a FLUOstar Omega spectrophotometer (BMG Labtech, Cary, NC) corrected for a blank of PIB containing identical reagents and incubation procedures minus cells. Cells were washed, lysed, and their protein content quantified. Experimental absorbance readings were extrapolated onto a ferrozine-Fe^{II} standard curve was used to convert experimental absorbance reading into the amount of Fe^{II} present in solution. These values were normalized for protein content.

^{59}Fe-transferrin loading procedure

The loading of ^{59}Fe onto Tf was performed as previously described (Burdo et al. 2003) with modifications. Briefly, using Tf-loading buffer (0.1 M HEPES, pH 7.5, 0.15 M NaCl), 20 mM $NaHCO_3$, 21.3 mM NTA, 44 μM ^{59}Fe, and 20 μM apo-Tf we did the following. ^{59}Fe was incubated with Tf-loading buffer containing $NaHCO_3$ and NTA for 5 min at RT after which apo-Tf was added and incubated for 2 h at RT. This ^{59}Fe-Tf solution containing non-Tf bound ^{59}Fe was buffer exchanged using a Nanosep 10 K MWCO Omega spin column (PALL Corporation, Port Washington, NY) 3 × 10 min at 5,500 rpm. This procedure yielded a ^{59}Fe-Tf purity of >95 %.

^{59}Fe uptake assays

All assays were performed in a 24-well tissue culture dish with a total working volume of 150 μl. Assay conditions were 1 h at 37 °C 5 % CO_2 shaking 120 rpm. Control assays, accounting for cell-associated ^{59}Fe, were performed at 4 °C 120 rpm. The radionuclide $^{59}FeCl_3$ was purchased from Perkin-Elmer, Waltham, MA. In all assays 1.0 μM ^{59}Fe was used regardless of its speciation, unless indicated otherwise. Reagent concentrations, where applicable, are as follows: 1 mM ferrozine, 100 μM Pt^{II}, 7.5 mM NH_4Cl, and 250 μM citrate. Citrate was added to all uptake and kinetic assays. Cells were pre-incubated with all assay reagents excluding the ^{59}Fe substrate for 30 min after which ^{59}Fe or ^{59}Fe-Tf were added. Each experiment was stopped after 1 h via consecutive washes with ice cold quench buffer (62.5 mM Tris, 12.8 mM EDTA (Thermo Fisher Scientific, Waltham, MA), 37.5 mM succinic acid (Sigma-Aldrich, St. Louis, MO). Cell monolayers were then lysed with 200 μl mammalian lysis buffer; 100 μl of this lysate were assayed for ^{59}Fe using a Wallac γ counter. The remaining 100 μl was used for quantification of protein content. Counts were converted to pmol ^{59}Fe using a ^{59}Fe standard curve. Total ^{59}Fe content/replicate was normalized for protein concentration. Each datum point from our ^{59}Fe-saturation or Mn/Zn competition assays was taken after 1 h incubation. For our saturation and competition experiments ^{59}Fe was kept in a reduced state by incubation with 2 mM ascorbate throughout the assay. This was done to make ^{59}Fe uptake reductase independent.

Quantification of protein concentration

The protein content of Caco-2 and hBMVEC were determined according to the method described by (Bradford (1976) using BSA as the standard.

Results

Identification of iron transport proteins in cultured hBMVEC

To begin our analysis of the iron-related proteins expressed by hBMVEC we confirmed the expression of both DMT1 and TfR. Using an immunoblot containing proteins purified from the membranes of both Caco-2 and hBMVEC, we probed for DMT1 with an antibody that is specific for exon 2 and found a strong band at ~62 kDa (Fig. 1e). Using indirect

immunofluorescence, we found that TfR in hBMVEC was plasma membrane-associated (Fig. 1a); our relatively low-resolution epifluorescence images precluded our visualizing endosomal TfR. Von-Willebrand factor (VWF), an endothelial cell-specific protein, was used as a marker for hBMVEC (Fig. 1b).

Next, we examined the expression of ferrireductases in hBMVEC. Probing for Dcytb via immunoblot, we identified Dcytb immunoreactive protein of ~40 kDa in both hBMVEC and Caco-2 cells as positive control (Fig. 1e). Strong bands were also identified at ~48 kDa when probed with an anti-STEAP2 antibody (Fig. 1e). We used indirect immunofluorescence to probe the sub-cellular localization of STEAP2 in hBMVEC and found the protein to localize to the plasma membrane (Fig. 1c); again our relatively low-resolution epifluorescence images precluded our visualizing endosomal STEAP2. Plasma membrane localization of STEAP2 occurs in cells expressing the endothelial cell-specific marker VWF (Fig. 1d). Full-length western blots displayed little to no background when using antibodies from Fig. 1e, indicating a high degree of specificity (Supplementary Fig. 1). These data present novel evidence for the expression of the ferrireductases STEAP2 and Dcytb in hBMVEC.

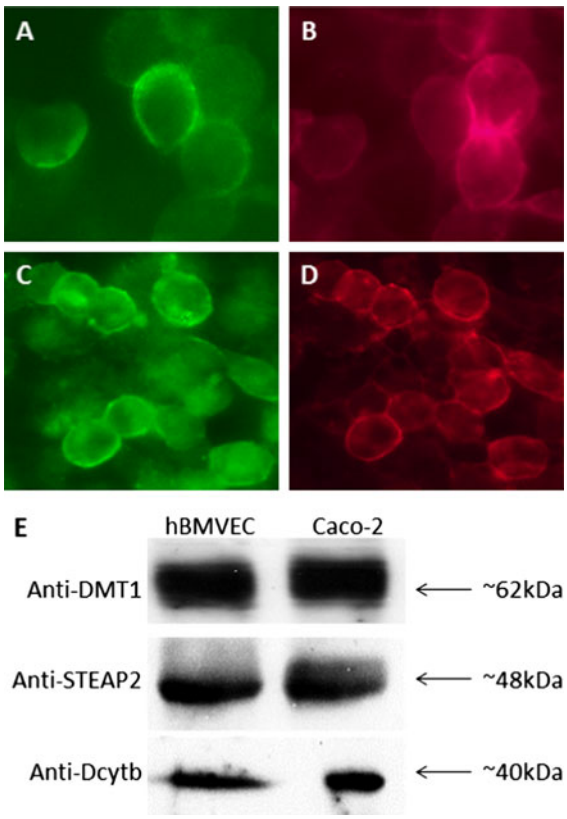

Fig. 1 TfR, DMT1, STEAP2, and Dcytb expression in hBMVEC. Indirect immunofluorescence was carried out using hBMVEC monolayers. Co-immunofluorescence yields localization of both TfR and VWF to the plasma membrane (**a** and **b**, respectively) (40× magnification). The same is true for STEAP2 and VWF (**c** and **d**, respectively) (40× magnification). Immunoblot's were carried out with proteins purified from the membranes (DMT1) or from whole cell lysates (STEAP2 & Dcytb) of the respective cell types as indicated (**e**). Antibodies used are as indicated to the left of the blots and size in kDa to the right

Reduction of iron from Tf is dependent upon citrate and TfR

Monolayers of hBMVEC were incubated with holo-Tf, ferrozine, and increasing amounts of citrate. Increasing the citrate concentration yielded an increased reduction of iron from Tf as measured by the formation of ferrozine-Fe^{II} complex (Fig. 2a). The inhibition of Tf, TfR interactions at the hBMVEC surface by either anti-TfR antibody or tenfold excess of apo-Tf significantly inhibited the reduction of iron from Tf (Fig. 2b, c respectively). These data show that hBMVEC can reduce iron from Tf and this hBMVEC-dependent reduction is dependent upon citrate concentration and the interaction of Tf with endogenous TfR.

Cell-surface ferrireductases are required for the hBMVEC-dependent reduction of TBI and NTBI

We used Pt^{II}, an inhibitor of pyridine nucleotide-dependent reductases (Armarego and Ohnishi 1987) including cell-surface ferrireductases (Eide et al. 1992), to assess the relative contributions of ferrireductases in mediating the reduction of TBI and NTBI. Dose–response experiments indicated that 100 μM Pt^{II} exihibited minimal cytotoxicity in hBMVEC monolayers (Supplementary Table 1) while displaying maximal effectiveness in inhibition of ferrireduction by hBMVEC (data not shown). The addition of 100 μM Pt^{II} to the hBMVEC monolayer significantly inhibited reduction of iron from Tf (Fig. 3a). In contrast, the addition of 100 μM Pt^{II} did not significantly inhibit the reduction of NTBI (Fig. 3b).

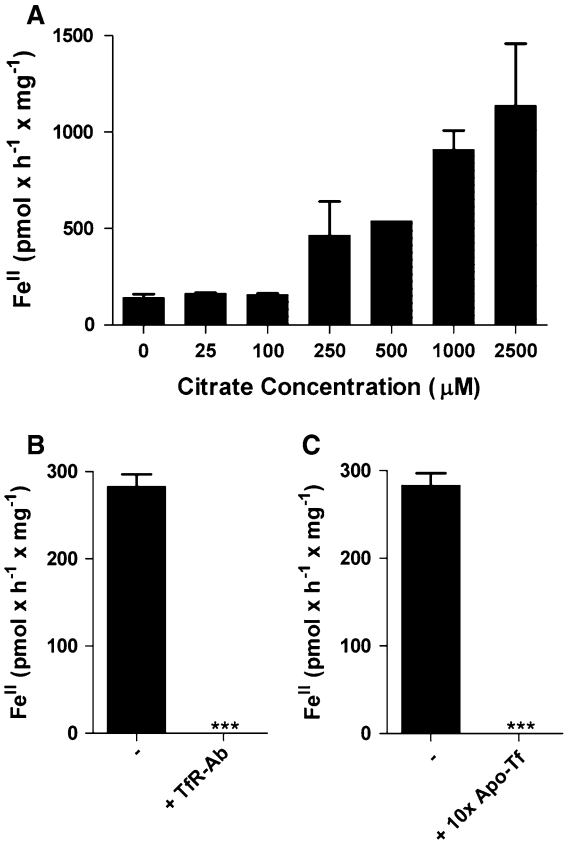

Fig. 2 Reduction of TBI is dependent upon citrate concentration and Tf-TfR interaction. The hBMVEC-dependent formation of Fe^{II} species were quantified using colorimetric ferrozine assays. Each sample was blank corrected with a minus hBMVEC control and normalized for protein concentration. Monolayers of hBMVEC were incubated with TBI, ferrozine, and either increasing concentrations of citrate (**a**), anti-TfR antibody (**b**), or tenfold apo-Tf (250 μM) (**c**). (**b, c**) contained a constant citrate concentration. $n = 3$ for each result in each panel. Data are mean ± standard deviation (SD). ***P-value <0.0001 as analyzed by the paired t-test

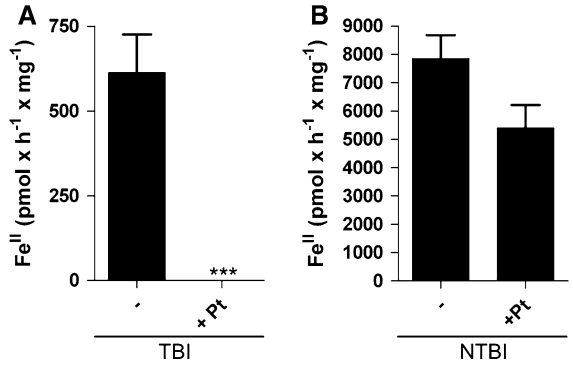

Fig. 3 Reduction of TBI and NTBI is dependent upon hBMVEC-surface ferrireductases. Colorimetric ferrozine assays were used to quantify the formation of Fe^{II} species in solution. Each sample was blank corrected with a minus hBMVEC control and normalized for protein concentration. Potassium tetrachloroplatinate^{II} (100 μM) was used to inhibit reductase activity by hBMVEC. Substrates were either TBI (**a**) or NTBI (**b**). Values are mean ± SD (a, n = 12; b, n = 3). ***P-value ≤0.0001 as analyzed by the paired t-test

hBMVEC can accumulate ^{59}Fe from TBI and NTBI

Fe^{II} released and reduced from Tf or exogenous ligand (e.g. citrate) is likely substrate for hBMVEC divalent cation transporter(s) at the plasma membrane. We monitored the uptake of iron into hBMVEC through the use of the radionuclide ^{59}Fe using either ^{59}Fe-NTBI (^{59}NTBI) or ^{59}Fe-TBI (^{59}TBI). Monolayers of hBMVEC accumulate ^{59}Fe with $^{59}Fe^{II}$-citrate as substrate (reductase-independent uptake conducted in the presence of 2 mM dihydroascorbate). Under these conditions, hBMVEC accumulate iron with a $K_M = 3.9 \pm 1.1$ μM (Fig. 4a). Using ^{59}TBI as substrate without added Asc (reductase-dependent) we tested the postulate that a Fe^{II} transporter is involved in TBI uptake. We used ferrozine to specifically inhibit accumulation of $^{59}Fe^{II}$ from ^{59}TBI. Ferrozine will chelate any free ferrous iron thus preventing the translocation into the cell of $^{59}Fe^{II}$ released from ^{59}Fe-Tf by ferrireduction. In this assay, ferrozine inhibited reductase-dependent iron uptake by approx. 50 % (Fig. 4b).

Pt^{II} was used to correlate ferrireductase inhibition with iron uptake inhibition. Uptake of ^{59}TBI by hBMVEC was quantified in the presence of Pt^{II} (Fig. 4c). The remaining cell-associated ^{59}Fe in Figs. 4b and 4c can be attributed to residual ^{59}TBI-TfR interactions, the quantities of which are comparable to 4 °C controls (141.1 ± 10.5 pmol × h^{-1} × mg^{-1}; data not shown). Pt^{II} had no effect on $^{59}Fe^{II}$ uptake when ^{59}NTBI was used as substrate (Fig. 4d) suggesting that a cell-surface Pt^{II}-insensitive ferrireductase is involved in ^{59}NTBI uptake by hBMVEC. The data from Fig. 4d parallel our reductase assay results given in Fig. 3b.

Acidification is not required for the accumulation of TBI by hBMVEC

To assess the contribution made by canonical TfR cycling we performed alkalinization assays. Alkalinization

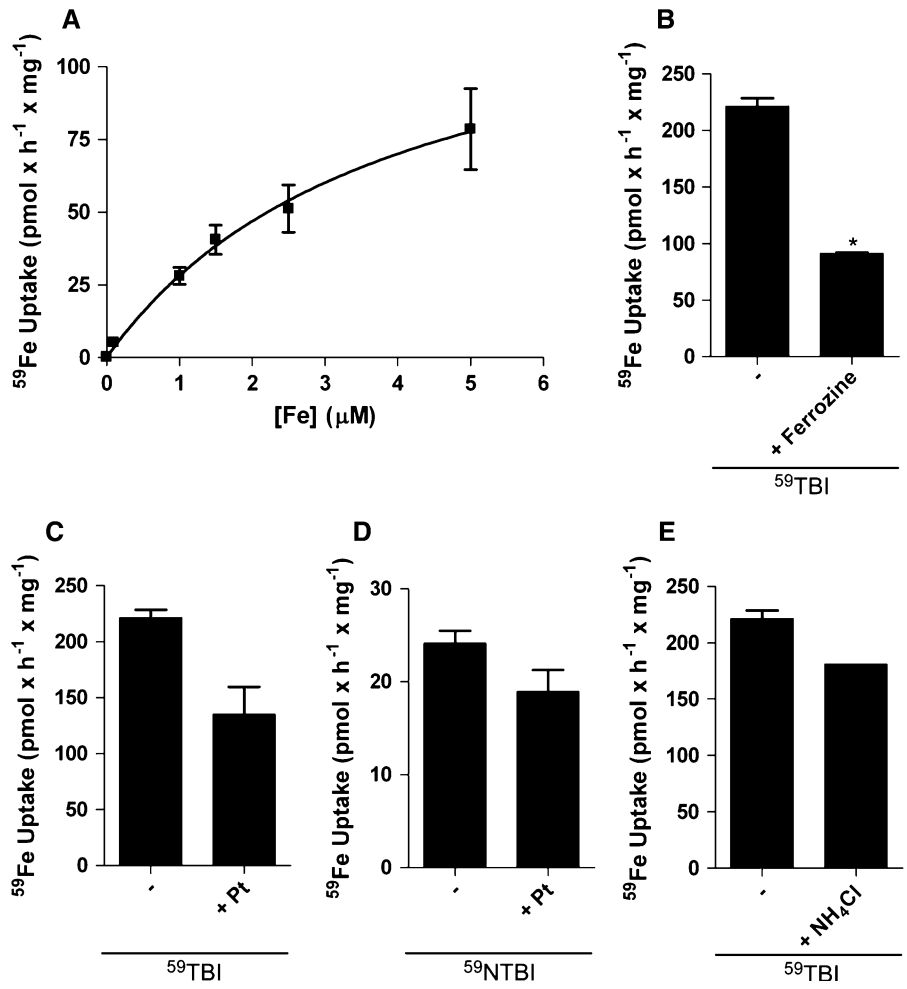

Fig. 4 Both TBI and NTBI are substrate for endosomal-independent hBMVEC iron uptake. A γ counter was used to quantify the amount of ^{59}Fe uptake by hBMVEC monolayers. The kinetics of $^{59}Fe^{II}$-citrate plus Asc accumulation by hBMVEC are shown (**a**). Data are shown representing hBMVEC accumulation of ^{59}Fe from ^{59}Fe-Tf in the presence ferrozine (**b**) or Pt^{II} (**c**). ^{59}NTBI uptake in the presence of Pt^{II} was also monitored (**d**). Effect of hBMVEC-alkalinization via NH_4Cl on ^{59}TBI accumulation was quantified and compared to control (**e**). n = 3 for each result in each panel. The Michaelis–Menten equation was used to calculate the curve (a). Data are mean ± SD. **P*-value ≤0.01 as analyzed by the unpaired *t*-test

assays using NH_4Cl inhibit proton accumulation in the endosomes, thus minimizing the proton-dependent mobilization of TBI and subsequent accumulation of iron. The data from the NH_4Cl alkalinization assay are depicted in Fig. 4e; the results demonstrate that hBMVEC uptake of ^{59}Fe from ^{59}TBI is not dependent on endosomal acidification and, therefore, likely not strongly dependent on canonical Tf-TfR cycling.

Iron accumulation by hBMVEC can be partially inhibited by Mn^{II} and Zn^{II}

Divalent cation transporters often transport several different metal ions which can compete with one another for uptake (Garrick et al. 2006a). Therefore, we used Mn^{II} and Zn^{II} in an attempt to inhibit $^{59}Fe^{II}$ translocation in a reductase-independent protocol (+Asc). Mn^{II} inhibited $^{59}Fe^{II}$ uptake into hBMVEC by ~50 % at both 0.1 μM and 1.0 μM $^{59}Fe^{II}$ concentrations; $IC_{50} = 4.3 \pm 1.2$ μM and 8.4 ± 2.5 μM (Fig. 5a, b respectively). Zn^{II} also inhibited $^{59}Fe^{II}$ accumulation by ~50 % with an $IC_{50} = 3.1 \pm 0.7$ μM (Fig. 5c). By quantifying this competition in the presence of both divalent cations we tested the hypothesis that two separate divalent cation transporters were functioning in hBMVEC, one specific for Mn^{II}, the other specific for Zn^{II}. However, inclusion of Mn^{II} and Zn^{II} together at 50 μM each in the uptake buffer resulted in the equivalent 50 % inhibition of $^{59}Fe^{II}$ accumulation seen with either metal ion alone (Fig. 5d).

Discussion

The identification of the major iron transport proteins in hBMVEC is required for an understanding of the

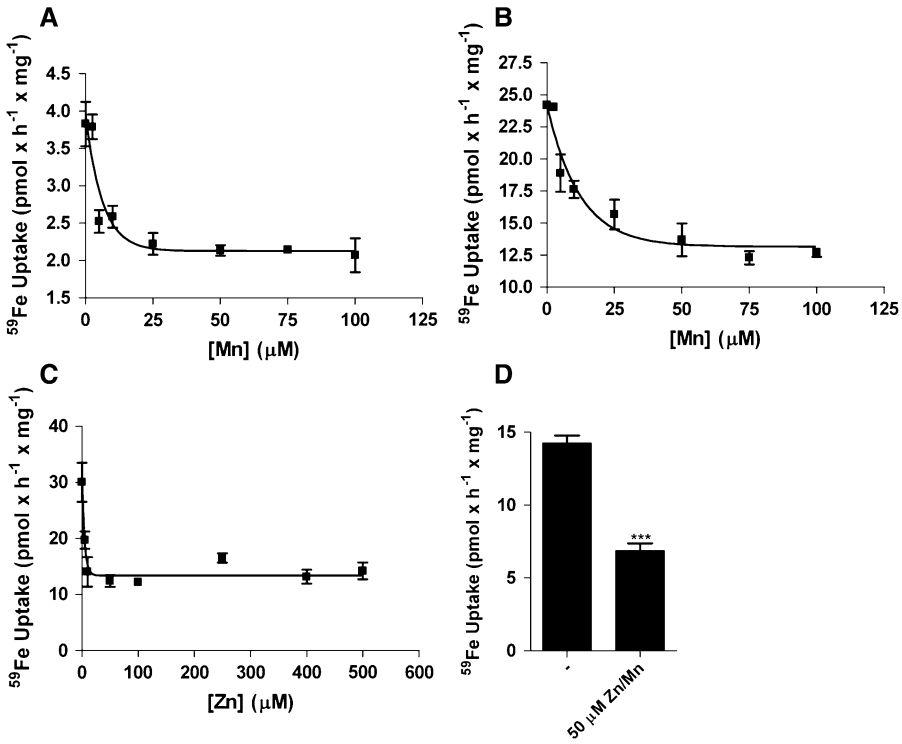

Fig. 5 Mn^{II} and Zn^{II} partially inhibit the uptake of ferrous iron by hBMVEC. A γ counter was used to quantify the amount of $^{59}Fe^{II}$-citrate plus Asc uptake by hBMVEC monolayers. Manganese^{II} inhibition of $^{59}Fe^{II}$-citrate plus Asc accumulation using either 0.1 μM ^{59}Fe (**a**) or 1.0 μM ^{59}Fe (**b**) as substrate. Zinc^{II} inhibition of 1.0 μM $^{59}Fe^{II}$-citrate plus Asc is shown (**c**). Combined Zn^{II} and Mn^{II} inhibition of 1.0 μM $^{59}Fe^{II}$-citrate plus Asc is shown (**d**). n = 3 for each result in each panel with the exception of (d) where $n = 6$. *Curves* were obtained using a one phase exponential decay equation. Data are mean ± SD. ***P-value ≤0.0001 as analyzed by the paired t-test

mechanisms regulating TBI and NTBI uptake at the BBB. Both TfR and DMT1 have been identified in rat brain microvessels by indirect immunofluorescence (Burdo et al. 2001). These workers also showed TfR and DMT1 co-localization in this tissue. Figure 1 corroborates this report regarding the expression of both TfR and DMT1 by the brain microvasculature. Further investigation using confocal microscopy would provide the necessary resolution to localize these proteins to specific hBMVEC compartments although our lower-resolution images do indicate their expression at the PM.

The reduction of Fe^{III} in Tf, and thus Fe dissociation, requires an increase in the reduction potential (E°) of Fe^{III} in the Fe^{III}–Tf complex which is <−500 mV at pH 7 (Kraiter et al. 1998). The E° of TBI increases when 1) Tf associates with TfR, 2) an exogenous ligand is presented in solution (i.e. citrate), or 3) when the pH of the solution becomes more acidic. For example, upon Tf binding to TfR, the Fe^{III} potential is increased by >200 mV (Dhungana et al. 2004). Electron transfer from endogenous reductants (i.e. NADH) to TBI are thermodynamically favorable when the E° of TBI becomes more positive than the E° of the endogenous reductants (Dhungana et al. 2004). Cell-surface ferrireductases channel these reducing equivalents from intracellular reductants through the plasma membrane to TBI and NTBI. In relation to the STEAP family of metalloreductases, Steap2 is highly expressed in the brain and co-localizes with TfR; these observations make Steap2 a likely hBMVEC ferrireductase candidate (Ohgami et al. 2006). Given the presence of STEAP2 (Ohgami et al. 2006) as well as Dcytb (Tulpule et al. 2010) transcripts in the brain, we assessed the expression of these two ferrireductases in hBMVEC specifically. The immunoblots (Fig. 1e) indicated that both Dcytb and STEAP2 are present in these cells. Redundancy in function is not unexpected for the BBB; there is evidence for such redundancy in Steap3 K/O mice which retain residual erythroid reductase activity (Ohgami et al. 2005). We demonstrated also a plasma membrane localization of Steap2 in hBMVEC (Fig. 1c), indicating its potential to act as a cell-surface ferrireductase in this cell type. Further investigation using confocal microscopy would be beneficial in identifying Steap2 in endosomal compartments.

Our data demonstrated that in the presence of citrate hBMVEC can reduce Tf-bound Fe^{III} at neutral pH. This result is consistent with literature data

indicating that both high citrate concentrations and Tf–TfR interactions increase the E° of Tf-associated Fe^{III} (Weaver et al. 2010; Dhungana et al. 2004; Bates et al. 1967). Citrate is a physiologically relevant ligand in the blood with reported concentrations ranging from 90 μM (Bradbury 1997; Gaasch et al. 2007) to 110 μM (Wolcott and Boyer 1948; Königsberger et al. 2000). As Tf in the blood, at a concentration of 25 μM, is only 30 % saturated with Fe^{III} the physiological ratio of Tf:citrate is roughly 1:13 (Vincent and Love 2011). Upon titration with 250 uM citrate (Tf:citrate ratio of 1:10) a significant increase in the reduction of TBI by hBMVEC was observed (Fig. 2a). At physiological concentrations the exogenous ligand citrate likely increases the E° of TBI allowing iron to be reduced from Tf by our hBMVEC (Fig. 2a). In addition, the data in Fig. 2b, c are consistent with observations that the Tf, TfR interaction alters the coordination of the Fe^{III} in such a way as to raise its E° allowing for reduction (Dhungana et al. 2004).

Next, we wanted to investigate the hypothesis that cell-surface ferrireductases are actively reducing TBI and/or NTBI. The Kaplan lab demonstrated that Fre1, a cell-surface ferrireductase found in *Saccharomyces cerevisiae*, is inhibited by Pt^{II} (Eide et al. 1992): Pt^{II} had previously been demonstrated to inhibit pyridine-nucleotide reductases likely by reaction with protein cysteine thiol(s) (Armarego and Ohnishi 1987). We extended these observations regarding Pt^{II} to our mammalian cell culture system and demonstrated that Pt^{II} effectively inhibited cell-surface reduction of TBI (Fig. 3a). In contrast, Pt^{II} had no effect on NTBI reduction by hBMVEC (Fig. 3b). We propose that in hBMVEC a Pt^{II}-sensitive cell-surface ferrireductase is required for the reduction of TBI while a Pt^{II}-insensitive one is responsible for Fe^{III} reduction (and release) in NTBI. This apparent difference in reductase sensitivity to Pt^{II} is under current investigation; note, however, that while Dcytb and the Steap proteins share ferrireductase activity, they are neither genetic nor structural homologs.

Since TBI and NTBI appear reduced at the cell-surface of hBMVEC, we hypothesized that the substrate for hBMVEC iron accumulation would be Fe^{II}. To test this we conducted a reductase-independent NTBI $^{59}Fe^{II}$-uptake analysis with hBMVEC monolayers (Fig. 4a). Our results indicate that hBMVEC accumulate $^{59}Fe^{II}$ with a K_M value ~3.9 μM similar to the value for DMT1 expressed in HEK293 cells, ~3 μM (Garrick et al. 2006a). To investigate whether Fe^{II} reduced from Tf was acting as substrate for hBMVEC iron uptake we incubated hBMVEC with ^{59}TBI and ferrozine. Our results showed that ferrozine significantly inhibited the uptake of $^{59}Fe^{II}$ from TBI into hBMVEC (Fig. 4b), suggesting that Fe^{II} reduced from Tf is substrate for uptake at the PM of hBMVEC. We interpret residual ^{59}Fe accumulation by hBMVEC in the presence of ferrozine as "cell-associated iron"; that is, $^{59}Fe^{III}$ most probably in complex with Tf-TfR. Further examination of this inference is ongoing.

We sought to correlate the Pt^{II} inhibition of Fe^{III} reductase activity with an inhibition of $^{59}Fe^{III}$ uptake. Unlike in our reductase assays, we detected no significant difference in the uptake of either ^{59}TBI or ^{59}NTBI when Pt^{II} was present (Fig. 4c, d respectively). The relative effectiveness of Pt^{II} inhibition on iron uptake differs from what we see regarding the Pt^{II} effect on reduction (Fig. 3a). The residual ^{59}Fe accounted for in the presence of Pt^{II} is consistent with what is seen when ferrozine is present (Fig. 4b). Taken together, when "cell-associated" ^{59}Fe is accounted for, these data indicate that Pt^{II} inhibits ^{59}TBI uptake in hBMVEC. We must assume that "cell-associated" ^{59}Fe also exists in our controls resulting in significantly less ^{59}Fe uptake in comparison to Fe^{II} produced from reduction by hBMVEC. Thus, we infer from our data that Fe^{III} reduction is not the rate-limiting step in iron accumulation by hBMVEC. This inference is consistent with the fact that overall Fe^{III} reduction in 3 h was 3.5-fold greater than the corresponding ^{59}Fe-uptake in the same time period, or twofold greater if not accounting for residual "cell-associated" ^{59}Fe.

In canonical Tf-TfR endosomal cycling, the dissociation and reduction of iron from Tf is partially mediated by endosomal acidification. Furthermore, transport of Fe^{II} through DMT1 has a pH optimum of 5.5 and involves an inward proton current that is coupled to iron translocation (Gunshin et al. 1997). With these facts in mind, we performed an alkalinization assay to determine if acidification contributes to the accumulation of iron by hBMVEC. The data in Fig. 4e demonstrate that an alkaline environment is not inhibitory to accumulation of iron from Tf indicating that cell-surface and/or endosomal acidification does not contribute the ^{59}Fe accumulation we observe. We conclude that canonical Tf-TfR endosomal cycling does not make a quantitatively significant contribution to the ^{59}TBI uptake in this cell

system as this mechanism is enhanced by endosomal acidification (Steere et al. 2010; Byrne et al. 2010).

DMT1 has a broad substrate range which includes Fe^{II}, Mn^{II}, and Zn^{II}; reciprocally, Mn^{II} and Zn^{II} can inhibit Fe^{II} transport by DMT1 (Gunshin et al. 1997; Garrick et al. 2006a; Roth et al. 2002). We assessed the activity of Mn^{II} and Zn^{II} as inhibitors of $^{59}Fe^{II}$ uptake by hBMVEC. We demonstrated that the separate and simultaneous competition with each metal inhibited the accumulation of iron by hBMVEC by $\sim$50 % (Fig. 5a–d), that is, both ions inhibited but their actions were neither additive nor synergistic. We propose, therefore, that at least two divalent cation transporters are expressed at the hBMVEC PM: a Fe^{II}, Mn^{II}, and Zn^{II} transporter and a Fe^{II}-specific one that is insensitive to Mn^{II} or Zn^{II}. We calculated an IC_{50} for each cation to provide an estimate of the kinetic K_M they might have as substrates. This IC_{50} for Mn^{II} was 8.4 ± 2.5 μM whereas the value for Zn^{II} was 3.1 ± 0.7 μM (Fig. 5e–f). Application of the Cheng-Prusoff equation to these IC_{50} values (Biochem Pharm 1973; Cer et al. 2009) provided estimates for K_I values; these were: Mn, 8.4 μM; Zn, 3.1 μM. These values do not correlate with K_M values for Mn^{II} and Zn^{II} in the uptake of these divalent metal ions by DMT1; the K_M value for Mn^{II} is $\sim$1 μM (Garrick et al. 2006a) while this value for Zn^{II} is $\sim$42 μM (Iyengar 2009). Therefore, we suggest a Fe^{II} transporter other than DMT1 contributes significantly to ferrous iron uptake by hBMVEC. One candidate for this activity is Zip14 which has been identified at the mRNA level in the CNS (Bishop et al. 2010; Girijashanker et al. 2008). We are currently testing this hypothesis.

Acknowledgments We thank Dr. Supriya Mahajan for her generous gift of hBMVEC. This work was supported by a grant from the National Institute of Health and a fellowship from the American Heart Association.

References

Abbott NJ, Ronnback L, Hansson E (2006) Astrocyte–endothelial interactions at the blood-brain barrier. Nat Rev Neurosci 7(1):41–53

Armarego WLF, Ohnishi A (1987) Inactivation of dihydropteridine reductase (human brain) by platinum (II) complexes. Eur J Biochem 164(2):403–409. doi:10.1111/j.1432-1033.1987.tb11072.x

Atanasova B, Mudway IS, Laftah AH, Latunde-Dada GO, Mckie AT, Peters TJ, Tzatchev KN, Simpson RJ (2004) Duodenal ascorbate levels are changed in mice with altered iron metabolism. J Nutr 134(3):501–505

Bates GW, Billups C, Saltman P (1967) The kinetics and mechanism of iron(III) exchange between chelates and transferrin. J Biol Chem 242(12):2810–2815

Bishop G, Scheiber I, Dringen R, Robinson S (2010) Synergistic accumulation of iron and zinc by cultured astrocytes. Journal of Neural Transmission 117(7):809–817. doi:10.1007/s00702-010-0420-9

Bradbury MWB (1997) Transport of Iron in the Blood-Brain-Cerebrospinal Fluid System. J Neurochem 69(2):443–454. doi:10.1046/j.1471-4159.1997.69020443.x

Bradford MM (1976) A rapid and sensitive method for the quantitation of microgram quantities of protein utilizing the principle of protein-dye binding. Anal Biochem 72(1–2):248–254. doi:10.1016/0003-2697(76)90527-3

Burdo J, Menzies S, Simpson I, Garrick L, Garrick M, Dolan K, Haile D, Beard J, Connor J (2001) Distribution of divalent metal transporter 1 and metal transport protein 1 in the normal and Belgrade rat. J Neurosci Res 66(6):1198–1207. doi:10.1002/jnr.1256

Burdo JR, Antonetti DA, Wolpert EB, Connor JR (2003) Mechanisms and regulation of transferrin and iron transport in a model blood-brain barrier system. Neuroscience 121(4):883–890. doi:10.1016/s0306-4522(03)00590-6

Byrne SL, Chasteen ND, Steere AN, Mason AB (2010) The unique kinetics of iron release from transferrin: the role of receptor, lobe–lobe interactions, and salt at endosomal pH. J Mol Biol 396(1):130–140. doi:10.1016/j.jmb.2009.11.023

Dhungana S, Taboy CH, Zak O, Larvie M, Crumbliss AL, Aisen P (2004) Redox properties of human transferrin bound to its receptor†. Biochemistry 43(1):205–209. doi:10.1021/bi0353631

Eide D, Davis-Kaplan S, Jordan I, Sipe D, Kaplan J (1992) Regulation of iron uptake in Saccharomyces cerevisiae. The ferrireductase and Fe(II) transporter are regulated independently. J Biol Chem 267(29):20774–20781

Gaasch J, Lockman P, Geldenhuys W, Allen D, Van der Schyf C (2007) Brain iron toxicity: differential responses of astrocytes, neurons, and endothelial cells. Neurochem Res 32(7):1196–1208. doi:10.1007/s11064-007-9290-4

Garrick M (2011) Human iron transporters. Genes Nutr 6(1):45–54. doi:10.1007/s12263-010-0184-8

Garrick MDKH, Vargas F, Singleton S, Zhao L, Smith JJ, Paradkar P, Roth JA, Garrick LM (2006a) Comparison of mammalian cell lines expressing distinct isoforms of divalent metal transporter 1 in a tetracycline-regulated fashion. Biochem J 398(3):539–545

Garrick MD, Singleton ST, Vargas F, Kuo H-C, Zhao L, Knopfel M, Davidson T, Costa M, Paradkar P, Roth JA, Garrick LM (2006b) DMT1: Which metals does it transport? Biol Res 39:79–85

Girijashanker K, He L, Soleimani M, Reed JM, Li H, Liu Z, Wang B, Dalton TP, Nebert DW (2008) Slc39a14 Gene Encodes ZIP14, A Metal/Bicarbonate Symporter: Similarities to the ZIP8 Transporter. Mol Pharmacol 73(5):1413–1423. doi:10.1124/mol.107.043588

Gunshin H, Mackenzie B, Berger UV, Gunshin Y, Romero MF, Boron WF, Nussberger S, Gollan JL, Hediger MA (1997)

Cloning and characterization of a mammalian proton-coupled metal-ion transporter. Nature 388(6641):482–488
Königsberger LC, Königsberger E, May PM, Hefter GT (2000) Complexation of iron(III) and iron(II) by citrate. Implications for iron speciation in blood plasma. J Inorg Biochem 78(3):175–184. doi:10.1016/s0162-0134(99)00222-6
Kraiter DC, Zak O, Aisen P, Crumbliss AL (1998) A determination of the reduction potentials for diferric and C- and N-lobe monoferric transferrins at endosomal pH (5.8). Inorg Chem 37(5):964–968. doi:10.1021/ic970644g
Madsen E, Gitlin JD (2007) Copper and Iron Disorders of the Brain. Annu Rev Neurosci 30(1):317–337. doi:10.1146/annurev.neuro.30.051606.094232
Moos T, Nielsen TR, Skjørringe T, Morgan EH (2007) Iron trafficking inside the brain. J Neurochem 103(5):1730–1740
Ohgami RS, Campagna DR, Greer EL, Antiochos B, McDonald A, Chen J, Sharp JJ, Fujiwara Y, Barker JE, Fleming MD (2005) Identification of a ferrireductase required for efficient transferrin-dependent iron uptake in erythroid cells. Nat Genet 37(11):1264–1269. doi:10.1038/ng1658
Ohgami RS, Campagna DR, McDonald A, Fleming MD (2006) The Steap proteins are metalloreductases. Blood 108(4):1388–1394. doi:10.1182/blood-2006-02-003681
Rivera-Mancía S, Pérez-Neri I, Ríos C, Tristán-López L, Rivera-Espinosa L, Montes S (2010) The transition metals copper and iron in neurodegenerative diseases. Chem Biol Interact 186(2):184–199
Roth JA, Feng L, Dolan KG, Lis A, Garrick MD (2002) Effect of the iron chelator desferrioxamine on manganese-induced toxicity of rat pheochromocytoma (PC12) cells. J Neurosci Res 68(1):76–83. doi:10.1002/jnr.10207
Rouault TA, Cooperman S (2006) Brain iron metabolism. Semin Pediatr Neurol. 13(3):142–148
Salvador GA (2010) Iron in neuronal function and dysfunction. BioFactors 36(2):103–110
Siddappa AJM, Rao RB, Wobken JD, Leibold EA, Connor JR, Georgieff MK (2002) Developmental changes in the expression of iron regulatory proteins and iron transport proteins in the perinatal rat brain. J Neurosci Res 68(6):761–775. doi:10.1002/jnr.10246
Steere AN, Byrne SL, Chasteen ND, Mason AB Kinetics of iron release from transferrin bound to the transferrin receptor at endosomal pH. Biochimica et Biophysica Acta (BBA)—General Subjects (0). doi:10.1016/j.bbagen.2011.06.003
Steere A, Byrne S, Chasteen N, Smith V, MacGillivray R, Mason A (2010) Evidence that His349 acts as a pH-inducible switch to accelerate receptor-mediated iron release from the C-lobe of human transferrin. J Biol Inorg Chem 15(8):1341–1352. doi:10.1007/s00775-010-0694-2
Tulpule K, Robinson SR, Bishop GM, Dringen R (2010) Uptake of ferrous iron by cultured rat astrocytes. J Neurosci Res 88(3):563–571
Vincent JB, Love S (2011) The binding and transport of alternative metals by transferrin. Biochim Biophys Acta (BBA)—General Subjects (0). doi:10.1016/j.bbagen.2011.07.003
Weaver KD, Gabričević M, Anderson DS, Adhikari P, Mietzner TA, Crumbliss AL (2010) Role of citrate and phosphate anions in the mechanism of iron(III) sequestration by ferric binding protein: kinetic studies of the formation of the holoprotein of wild-type fbpa and its engineered mutants. Biochemistry 49(29):6021–6032. doi:10.1021/bi902231c
Wolcott GH, Boyer PD (1948) A colorimetric method for the determination of citric acid in blood and plasma. J Biol Chem 172(2):729–736
Yang W, Jung K, Lee M, Lee Y, Nakagawa S, Niwa M, Cho S, Kim D (2010) Transient expression of iron transport proteins in the capillary of the developing rat brain. Cellular and Molecular Neurobiology:1–7. doi:10.1007/s10571-010-9558-0